

Exploring the Programmable Assembly of a Polyoxometalate–Organic Hybrid via Metal Ion Coordination

Panchao Yin,[†] Tao Li,[‡] Ross S. Forgan,[§] Claire Lydon,[§] Xiaobing Zuo,[‡] Zhaoxiong Norm Zheng,[†] Byeongdu Lee,[‡] Deliang Long,[§] Leroy Cronin,^{*,§} and Tianbo Liu^{*,†,‡}

[†]Department of Chemistry, Lehigh University, Bethlehem, Pennsylvania 18015, United States

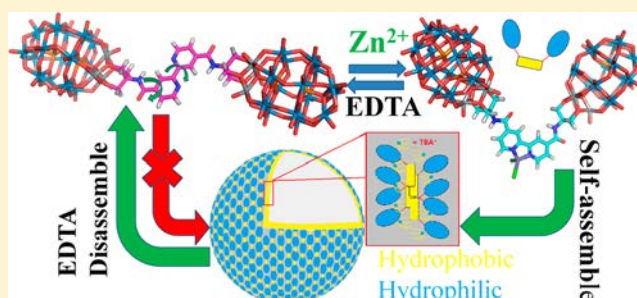
[‡]X-ray Science Division, Advanced Photon Source, Argonne National Laboratory, Argonne, Illinois 60439, United States

[§]WestCHEM, School of Chemistry, University of Glasgow, Glasgow G12 8QQ, U.K.

[‡]Department of Polymer Science, The University of Akron, Akron, Ohio 44325, United States

Supporting Information

ABSTRACT: The conformational flexibility and programmed assembly of a dumbbell-shaped polyoxometalate–organic hybrid molecule comprising two Dawson-type polyoxometalates linked by a 2,2′-bipyridine unit, which can be coordinate to metal ions, in this case of Zn^{2+} , are described. SAXS, UV/vis, and NMR spectroscopic techniques confirm that the hybrid molecules exist as the *trans* dumbbell in metal-ion-free solutions and can be reversibly transformed into the *cis* dumbbell through coordination upon the addition of $ZnCl_2$ into a DMSO solution containing the hybrid. Subsequent addition of EDTA reverses the switching process by extracting the Zn^{2+} cations from the hybrid. During the interchange process between *trans* and *cis* dumbbells, a further reorganization of the hybrid molecules occurs through bond rotation to minimize steric clashes between the polyoxometalate subunits, in order to stabilize the corresponding dumbbell conformation. The Zn^{2+} -controlled conformational transformation of the hybrid can be further utilized to manipulate the hybrid's solvophobic interaction-driven self-assembly behavior in the metal-ion driven reversible formation of 140 nm sized vesicles, studied by laser light scattering techniques.



INTRODUCTION

Molecular switches are molecules that can be reversibly shifted between two or more stable states in response to environmental stimuli, for example, pH, light, temperature, redox potential, electric field, and the presence of ligands or metal ions.^{1–14} In particular, the control of supramolecular assembly via metal ion coordination is a very useful approach to preparing artificial molecular switches^{13,15,16} and is vital in many biological behaviors, for example, metal ion-directed protein folding and self-assembly, Ca^{2+} induced contraction or relaxation of the human heart, Na^+ stimulated nerve impulses, and the Ca^{2+} -gated K^+ ion channel found inside cell membranes.^{17–20} It remains challenging, however, to build artificial metal-ion-driven molecular switches based on relatively simple molecules that operate on the tens of kilodaltons scale of proteins and demonstrate significant modification of self-assembly behavior. Molecular switches that respond to metal ion stimuli can suffer from the fact that complexation often only affects significantly the local area around the metal binding site, limiting the functionality of the switches. Moreover, molecular switches that display metal-ion-responsive folding and self-assembly behavior could be thought of as simple models to help us understand the corresponding biological process involving proteins and RNAs.

Polyoxometalates (POMs) are a large group of structurally well-defined molecular metal-oxide clusters (ca. 1–6 nm) with diverse physical properties and applications.^{21–24} Chemically grafting organic ligands or chains onto the POMs surface results in POM–organic hybrids, which can maintain, modify, or enhance the optical,^{25–27} electrical,^{28,29} thermal,³⁰ and fluorescence^{31–33} properties of the POMs. The functionality (e.g., self-assembly behavior and catalytic activity) of POM-based hybrids relies significantly on their molecular conformation, and therefore, POMs that exhibit conformational changes in response to external stimuli could be used as “switches” to enhance or remove these functions. Herein, we report, to the best of our knowledge, the first example of a POM-based metal-ion-driven molecular switch, which demonstrates a reversible switching process upon the coordination of Zn^{2+} cations. Moreover, during the interchange between the *trans* and *cis* dumbbells, a further reorganization of the hybrid molecules occurs through bond rotation to minimize steric clashes between the polyoxometalate subunits, in order to stabilize the corresponding dumbbell conformation. This controllable metal ion translocation is used to reversibly tune

Received: May 17, 2013

Published: August 9, 2013

the packing parameter of the POM-based hybrid (which can be treated as an amphiphile) and its consequent self-assembly behavior in the metal-ion driven reversible formation of 140 nm sized vesicles, as studied by laser light scattering (LLS) and TEM techniques. The working cycles of the molecular switch were also monitored by UV-vis and ^1H NMR spectroscopy, and the switching process was elucidated both by synchrotron small-angle X-ray scattering (SAXS) and 2D nuclear Overhauser effect spectroscopy (NOESY).

RESULTS AND DISCUSSION

Molecular Structure of the Hybrid Molecular Switch.

Hybrid **1**, $\text{TBA}_{10}\text{H}_2[\{\text{P}_2\text{V}_3\text{W}_{15}\text{O}_{59}(\text{OCH}_2)_3\text{NHCO}\}_2(\text{C}_5\text{H}_3\text{N})_2]$ (TBA, tetrabutylammonium), has been reported and fully characterized in a previous publication.³⁴ The hybrid has a dumbbell-like shape with the two Dawson-type POMs at opposite ends linked by a 2,2'-bipyridine unit, as evidenced by the crystal structure of a partially cation-exchanged sample (see Experimental Section for details) displayed in Figure 1. The

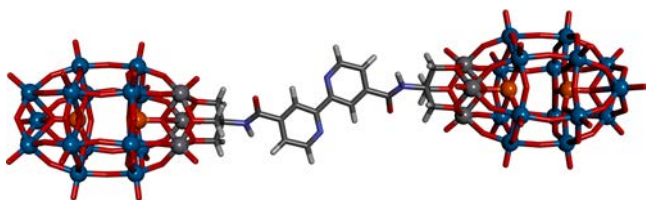


Figure 1. Representation of the molecular structure of the anionic component of hybrid **1**. Counterions and solvent molecules have been removed for clarity. Color code: W-blue, V-gray, P-orange spheres; C-gray, O-red, N-blue, H-white sticks.

covalent but nonconjugated linkage between the organic and inorganic building blocks of **1** ensures the molecule is quite stable while the functionalities of different components are maintained. The size of the molecule is ca. $1 \times 1 \times 4 \text{ nm}^3$, and it has a molecular weight of ca. 10.6 kDa. The 2,2'-bipyridine

unit has been explored with respect to incorporation into the design of switchable molecules because of the metal-ion-induced conformational rotation around the central C–C single bond, which occurs upon coordination of the metal ion.^{35–38} The purpose of designing hybrid **1** is to transfer the metal-ion-responsive behavior from the bipyridine unit to the hybrid POMs, study the interaction between the highly charged and bulky POM units in *trans* and *cis* dumbbell configurations, and control the hydrophobicity-driven self-assembly behavior through the introduction of metal ions. The POM units are connected to the 4,4' positions of the heteroaromatic rings, which not only can extend the bipyridine unit's conformation change to the entire hybrid molecule but also can attenuate somewhat the possible steric hindrance between the two POM units during the rotation process (Figure 2). Based on the above assumption, the hybrid can exist in two conformations: the *trans* dumbbell in a metal-ion-free environment, as illustrated in the solid-state structure, and the *cis* dumbbell driven by the coordination of the two nitrogen atoms of the central 2,2'-bipy unit to a metal ion.

UV/Vis Monitoring of the *Trans* to *Cis* Dumbbell Transformation Process. Titration of ZnCl_2 into a DMSO solution of the pure bipyridine ligand without POM attachments results in a classical bathochromic shift of the bipyridine-based absorption from λ_{max} of ca. 300 to 330 nm, which is attributed to the complexation between Zn^{2+} ions and the ligand (Figures S1 and S2 in Supporting Information). A resolved absorption peak for the bipyridine moiety is not observed in the UV/vis spectrum of hybrid **1**, because the strong absorption peak of the Dawson-type POM unit obscures it. Despite this, a similar bathochromic shift can be observed when Zn^{2+} is added to a DMSO solution of **1** (Figure 3). For a control titration experiment, ZnCl_2 is titrated against the dumbbell-shaped hybrid **2**,³⁹ which has an oxalate-based linker rather than a bipyridine one (Figure S3 and S4 in Supporting Information). It induces no obvious change in the UV/vis spectrum, ruling out the possibility that the interaction between the anionic POM subunit and Zn^{2+} ions contributes to the

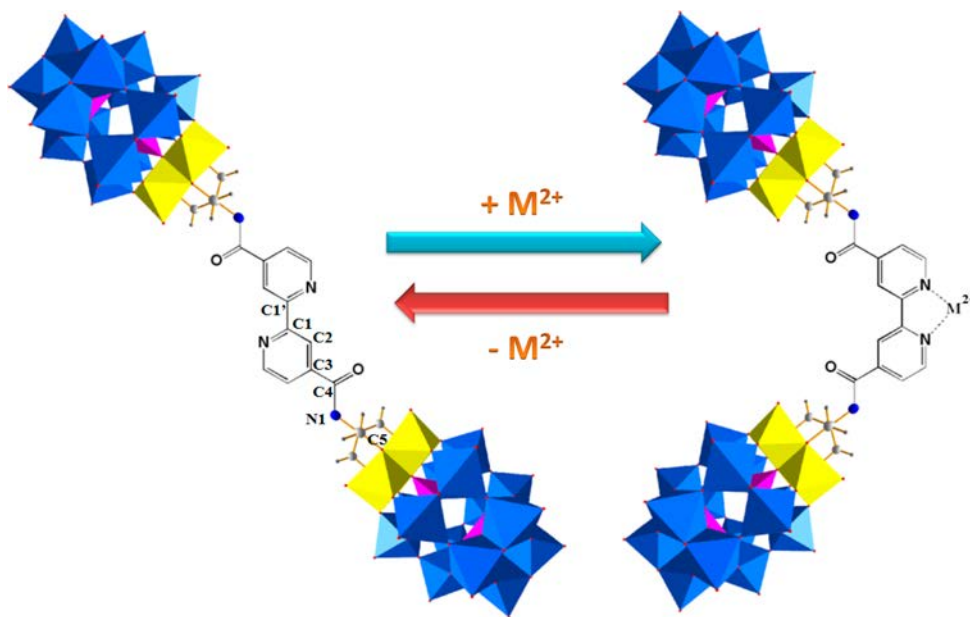


Figure 2. The reversible conformational transformation that occurs when **1** (denoted as the *trans* dumbbell herein) is complexed by a divalent metal chloride to form the complexed (*cis*) dumbbell.

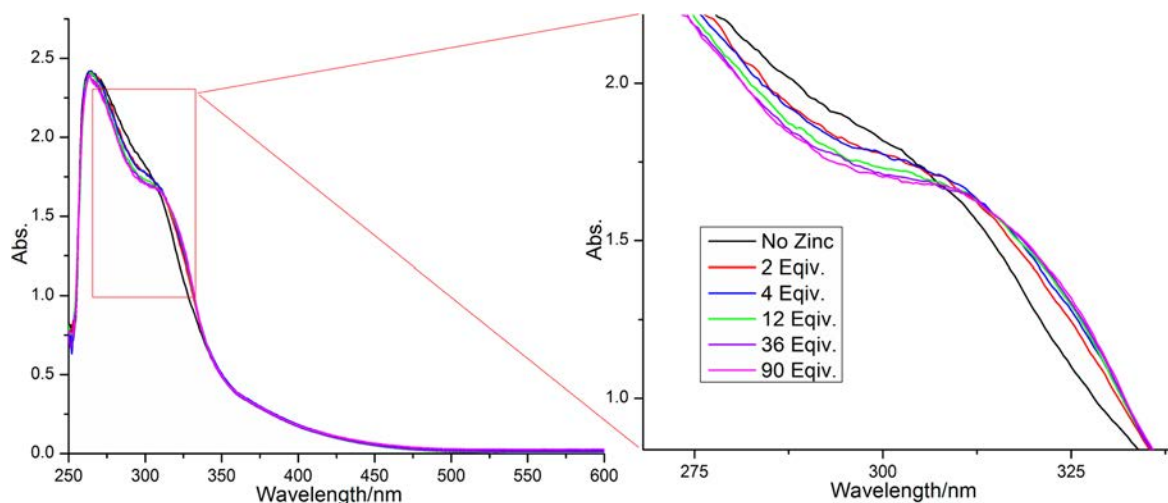


Figure 3. UV-vis spectroscopic monitoring of the titration of ZnCl_2 into a DMSO solution of hybrid **1**.

bathochromic shift. As a result, the addition of Zn^{2+} is expected to trigger the formation of a Zn-bipyridine complex and consequently change the conformation of the dumbbell structure from *trans* to *cis*.

^1H NMR Monitoring of the Reversible Transformation Process.

^1H NMR spectroscopy was used to obtain detailed information regarding the reversibility of the metal-ion-driven switching process. ^1H NMR spectroscopic studies in $\text{DMSO}-d_6$ on the bipyridine ligand without POM attachments show downfield shifts and broadening of the resonances associated with the heteroaromatic rings and amino groups in the spectrum of the ligand upon the addition of ZnCl_2 . The signal changes reach a maximum after the Zn^{2+} ions reach a molar ratio of 3.5:1 to bipyridine (i.e., 3.5 equiv; see Figure S5, Supporting Information). This peak shifting and broadening effect is characteristic of complexation. A similar phenomenon can be observed in the corresponding experiments (Figure 4) with hybrid **1**. After titration of larger amounts of ZnCl_2 into the hybrid solution (up to 40 equiv), the signals corresponding to H_a and H_c at 7.85 and 8.75 ppm, respectively, gradually decrease, coinciding with the appearance and growth of two new peaks at 8.15 and 9.05 ppm, indicating the Zn^{2+} -complexation controlled *trans* to *cis* transformation. Meanwhile, the peaks assigned to H_b and H_d , at 8.45 and 8.85 ppm, respectively, continuously move downfield to 8.55 and 8.90 ppm, respectively. As high as ca. 40 equiv of ZnCl_2 is needed to fully convert the *trans* dumbbell of hybrid **1** to the *cis* dumbbell, probably due to the repulsive interaction between the giant Dawson clusters during the rotation process. Interestingly, the downfield shifted peaks return to their original upfield positions after the addition of ca. 20 equiv of $(\text{TBA})_4\text{-EDTA}$ (tetra-*n*-butylammonium ethylenediaminetetraacetate, see Experimental Section), suggesting that the EDTA chelates the Zn^{2+} ions by extracting them from the *cis* dumbbell, which subsequently converts by rotation around the C–C bond to the *trans* dumbbell configuration. The addition of Zn^{2+} ions and their later removal with EDTA in the DMSO solution of hybrid **1** can be considered as a running cycle of a molecular switch (Figure 2). Further ^1H NMR spectroscopic studies confirm that the Zn^{2+} -controlled switching process occurs seamlessly for at least 5 cycles without decomposition of the hybrids or dysfunctionality (Figure S7 in Supporting Information).

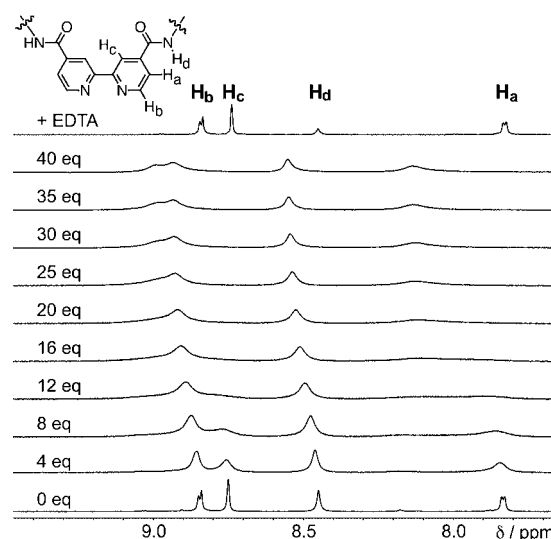


Figure 4. Stacked partial ^1H NMR spectra (500 MHz, $\text{DMSO}-d_6$, 298 K) covering the addition of 0–40 equiv of ZnCl_2 to 25 mg of the hybrid **1** dissolved in $\text{DMSO}-d_6$, showing signal broadening and shifting upon complexation of the Zn^{2+} to the bipyridine unit. The spectrum of the sample after subsequent addition of $(\text{TBA})_4\text{-EDTA}$ (top), which chelates the Zn^{2+} cations, shows signals commensurate with the metal-free hybrid. The assignment of the resonances in **1** was confirmed by a $^1\text{H}-^1\text{H}$ COSY spectrum (see Supporting Information).

Additionally, the *trans* to *cis* dumbbell transformation leads to an observable change in the diffusion speed of the hybrid molecule, as measured by 2D diffusion ordered ^1H NMR spectroscopy (DOSY). The DOSY results divulge diffusion coefficients (D) of $7.9 \times 10^{-11} \text{ m}^2 \text{ s}^{-1}$ for the *trans* dumbbell (before adding ZnCl_2) and $1.3 \times 10^{-10} \text{ m}^2 \text{ s}^{-1}$ for the *cis* dumbbell. Based on the Stokes–Einstein diffusion equation (equation provided in Experimental Section), the hydrodynamic radii (R_h) of the *trans* dumbbell and the *cis* dumbbell can be calculated as 1.4 and 0.8 nm, respectively. This observation could be explained by the shorter distance between two Dawson-type POMs in the *cis* dumbbell than in the *trans* dumbbell.

Observation of Coordination-Driven Switch by SAXS and NOESY. The molecular framework of hybrid **1** is

essentially rigid and only five single bonds are allowed to rotate (the pair of C4–N1, the pair of C3–C4, and C1–C1' in Figure 1 and 2); these bonds control the molecular conformation. However, due to the symmetrical structure of the Dawson-type POM, rotation of the pair of C5–N1 single bonds has no effect on changing the hybrid's conformation. The rotation of C1–C1' bond, and thus the *cis*–*trans* switch, highly relies on the complexation of the bipyridine chelating unit with metal ions. In addition, the C3–C4 bond is critical for the study of the coconformation of both the *trans* and the *cis* dumbbells. Our experimental results and the consideration of minimized energy of the dumbbell structure suggest that the amide groups and the neighboring heteroaromatic rings are expected to adopt a coplanar orientation because of the conjugative effect, which will limit the possible coconformations for both the *cis* dumbbell and the *trans* dumbbell to only three each (Figures 1 and 5 and discussions in Supporting Information). SAXS, a

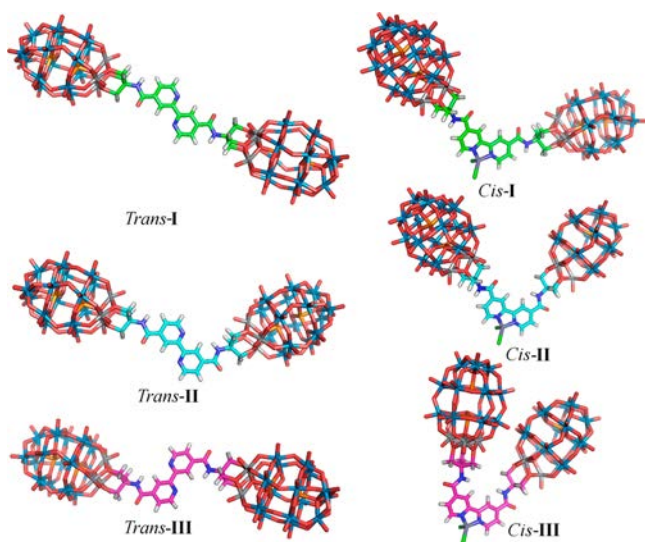


Figure 5. Calculated structures of the three possible coconformations that can be generated by rotation around the C3–C4 bonds for both the *trans* dumbbell (Zn-free) and *cis* dumbbell (Zn complex).

powerful technique for characterizing nanostructures in solution, was used to determine the coconformation of hybrid **1** in DMSO solution.^{40–44} The SAXS profiles of hybrid **1** before (open square) and after (open circle) adding ZnCl₂ (Figure 6) are remarkably different, exhibiting peak maxima at $q = 0.27$ and 0.33 \AA^{-1} , respectively (Figure 6a). Furthermore, the pair distance distribution functions (PDDF) in real space, $p(r)$, were obtained using the program GNOM⁴⁵ as shown in Figure 6b. All PDDFs exhibit a dumbbell-type bimodal feature, where the first peak describes the *intra*-subunit (Dawson-type POM) distances and is the same for both dumbbells, while the second peak describes the *inter*-subunit pair distances. The position of the second peak roughly measures the center to center distance of the two POM subunits of the dumbbell-shaped hybrid.⁴⁶ The second peak maximum is shifted from 28.5 to 21.2 Å after adding ZnCl₂, as a result of the metal-binding induced *trans* to *cis* switch; the POM subunit separation is considerably shorter in the *cis* dumbbell. In order to further probe the solution coconformations, the theoretical PDDF for each coconformation was calculated using the program SolX^{47,48} and superimposed upon the experimental PDDFs in Figure 6c. All three *trans* coconformations fit well with the experimental curve due

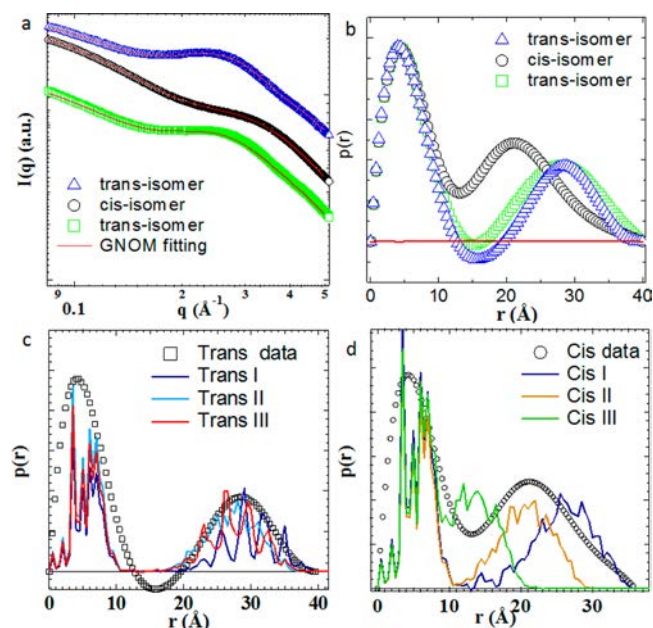


Figure 6. (a) SAXS curves of DMSO solutions of the metal-free *trans* dumbbell of **1** (open squares), the *cis* dumbbell generated after adding an excess of ZnCl₂ (open circles), and the *trans* dumbbell that is regenerated after adding TBA₄-EDTA to the solution containing the *cis* dumbbell (open triangles). The SAXS profiles are vertically offset for clarity. (b) Pair distance distribution functions (PDDFs) of the three samples obtained using the program GNOM. (c) The overlay of calculated PDDFs of the three possible *trans* coconformations and the experimentally derived PDDF of the *trans* dumbbell. The calculated PDDFs were computed directly from the molecular coordinates using the program SolX. (d) The overlay of calculated PDDFs of the three possible *cis* coconformations and the experimentally derived PDDF of the *cis* dumbbell.

to the similar subunit separations in each. For the *cis* dumbbell, however, the calculated PDDF for *cis*-II displays the best fit to the experimental data of the *cis* dumbbell solution, indicating that it is the most populated coconformation, with the probable slight shoulder at ca. 35 Å suggesting a small contribution from the other coconformations is possible, that is, the dumbbells exhibit some dynamic behavior in DMSO.

To further examine the coconformations, 2D NOESY NMR spectroscopic measurements were employed. Two-dimensional NOESY NMR spectroscopy can identify spins undergoing cross-relaxation and measure their cross-relaxation rates.⁴⁹ The intensity of NOESY cross-peaks are dependent on the distance between protons, and normally a signal is observed only if the corresponding proton–proton distance is $<5 \text{ \AA}$.⁴⁹ As such, NOESY experiments were expected to complement the SAXS studies by determining the extent of proton–proton interactions and the proximity of the organic fragments. The NOESY spectrum recorded at room temperature on a sample of **1** dissolved in DMSO-*d*₆, that is, the *trans* dumbbell, exhibited a much stronger correlation between the amido proton (H_d) and H_c compared with that between H_d and H_a, implying that *trans*-III is the major coconformation of the Zn-free hybrid in solution (Figures 5 and 7a), as opposed to the *trans*-I coconformation observed in our particular solid-state sample (Figure 1). In contrast, the NOESY spectrum of a DMSO solution of **1** with 40 equiv of ZnCl₂ added to induce full complexation (i.e., to form the *cis* dumbbell) exhibits significant correlations between H_d and both H_a and H_c. This

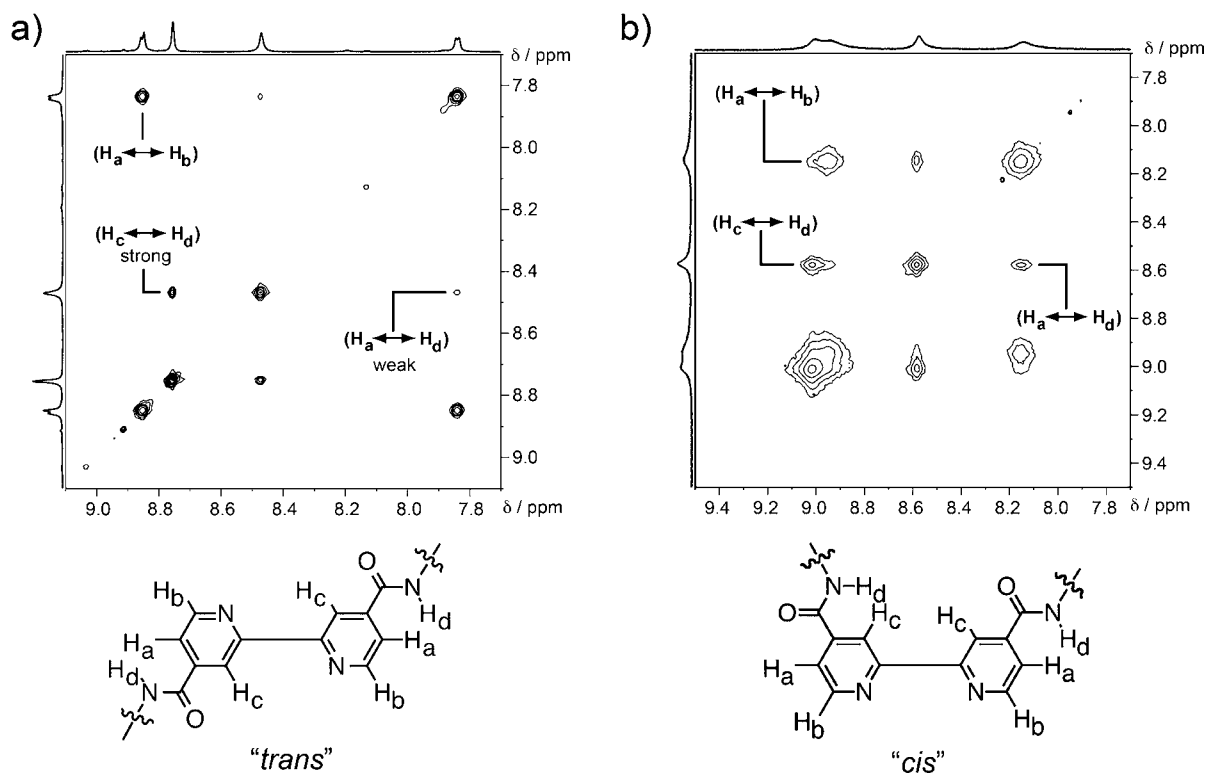


Figure 7. Labeled partial ^1H – ^1H NOESY NMR spectra (500 MHz, $\text{DMSO-}d_6$, 298 K) of (a) hybrid **1** without Zn^{2+} and (b) hybrid **1** with 40 equiv of ZnCl_2 added. The difference in relative strengths of the H_a – H_d and H_c – H_d correlation cross peaks indicates that **1** predominantly adopts the *trans*-III coconformation and, in the presence of Zn^{2+} , the *cis*-II coconformation, although dynamic exchange is possible. Structural diagrams for both dumbbells are given for guidance only, to show both possible orientations of the amide groups with respect to rotation around the C3–C4 bond, and the subsequent close contacts between protons.

observation appears to correlate well with the SAXS result, which suggests that *cis*-II is the major coconformation of the *cis* dumbbell solution (Figure 5 and 7b). It should be noted that *cis*-II has reduced symmetry and, as a result, we would expect the ^1H NMR spectrum to exhibit six resonances for the aromatic protons since all are heterotopic, but only three broad resonances are observed. We attribute this observation to the dynamic exchange between coconformations, through rotation of the C3–C4 bond, which is occurring fast on the NMR time scale and giving a spectrum that is the average of all coconformations of the *cis* dumbbells, major or minor, sampled in solution.

In theory, addition of ZnCl_2 to **1** to stimulate the rotation of the C1–C1' bond would change the expected major coconformation, *trans*-III, into *cis*-III if the C3–C4 bonds do not rotate. However, the inter-POM distance (center to center) in *cis*-III is quite short (1.2 nm), so steric hindrance/static charge repulsion is expected to be the driving force for one of the C3–C4 bonds to rotate by 180° and relieve this unfavorable strain by increasing the distance between the Dawson POM subunits to 2.0 nm (Figures 5 and 7c and video MV1 in Supporting Information). This further rotation of the C3–C4 bond could explain why a large excess of Zn^{2+} is required for the transformation from the *trans* to the *cis* dumbbell.

SAXS was also used to confirm that the *cis* dumbbell could be converted back to the *trans* dumbbell when the Zn^{2+} ions are removed from solution by the addition of a competing chelating agent. After addition of $(\text{TBA})_4\text{-EDTA}$ (shown in Figure 6a, open triangle), the d spacing increases to around ca.

28 Å, based on the $p(r)$ curve in Figure 6b (open square) indicating that the hybrids have reversibly changed back again to the *trans* dumbbell (Figure 7).

Metal-Ion-Driven Self-Assembly/Disassembly Behavior of Hybrid in Solution. It has been demonstrated previously that dumbbell-shaped hybrid POMs are amphiphilic molecules capable of forming vesicular nanostructures.^{39,50,51} The self-assembly behavior of amphiphilic surfactants is controlled by various factors especially their packing parameter (P), which is defined as $v_o/(a_e l_o)$, where v_o is the surfactant tail volume, l_o is the tail length, and a_e is the equilibrium area per molecule at the aggregate surface.^{52,53} In the current case, the metal-ion-driven conformational change of **1** was expected to alter its packing parameter (P), which might be utilized to manipulate its solvophobic-driven self-assembly behavior. The *trans* dumbbells, when dissolved in $\text{DMSO}/\text{methanol}$ (1:1 v/v) solution, exhibit a stable and low scattered intensity (ca. 40 kcps; scattered intensity for benzene is ca. 120 kcps) in time-resolved static light scattering (SLS) studies, suggesting that they exist as solvated single molecules. In contrast, the scattered intensity of this solution of **1** increased to ca. 9000 kcps, without any precipitation, after the addition of ca. 18 equiv of ZnCl_2 , suggesting the formation of large structures. A typical CONTIN analysis from a dynamic light scattering (DLS) study on these solutions indicated the existence of assemblies with an average R_h of 138 ± 7 nm and with a narrow size distribution (Figure 8a), only when Zn^{2+} is present. The average radius of gyration (R_g) of these assemblies that is obtained from the SLS measurement, 144 ± 7 nm, correlates closely with R_h , suggesting a hollow spherical vesicular structure for the

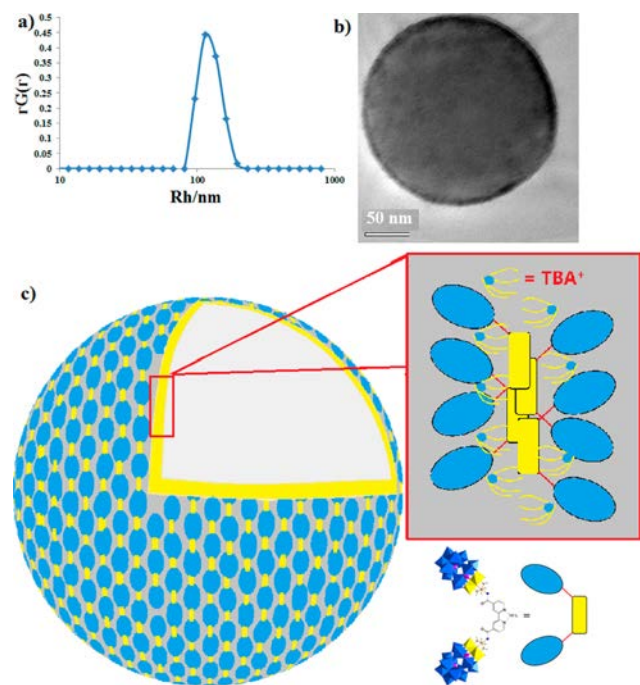


Figure 8. (a) DLS results of the assemblies of hybrid **1** in methanol/DMSO mixed solvents at 45° scattering angle. (b) TEM image of the large assembly. (c) The bilayer model for the vesicle structure.

assemblies. This observation is further confirmed by TEM studies (Figure 8b). By removal of ZnCl_2 from the *cis* dumbbell through the addition of $(\text{TBA})_4\cdot\text{EDTA}$, the conformation of **1** should change back to *trans* and the vesicles disassemble, as indicated by the drastic drop of the scattered intensity back to 47 kcps. This controllable self-assembly and disassembly process can be repeated with the same sample by adding and removing ZnCl_2 over several cycles (TOC graph and experimental details in Supporting Information).

A control experiment using the nonfunctional hybrid **2** shows that no large assemblies are observed, even after 54 equiv of Zn^{2+} ions is added (see experimental details in Supporting Information), which rules out the possibility that any POM subunit– ZnCl_2 interaction is the major driving force for the formation of these vesicular structures. The *trans* dumbbell of **1** is of approximately cylindrical shape with a diameter of ca. 1 nm; therefore the closest approach of the heteroaromatic rings in two adjacent hybrid molecules can be no less than 1 nm based on a parallel-packing model (see Figure S9 in Supporting Information).^{39,50} Since a distance of ca. 0.34 nm between the aromatic groups is necessary to form face-to-face π – π stacking contacts, it is difficult for the hydrophobic organic linkers of the *trans* dumbbell to directly interact with one another due to the steric hindrance of the larger POM subunits. In a previous study, the Zn-free (i.e., *trans* dumbbell) of **1** was observed to form vesicles in highly polar solvents (water/acetone mixtures) since the alkyl tails on the TBAs are expected to strongly interact with the organic linkers in these highly polar solvents and fill the solvophobic region.^{39,50} We expect that the interaction between the TBA cations and the organic linkers becomes weaker in comparatively less polar solvents, for example the DMSO/methanol mixtures utilized in this study, and therefore, no assemblies of the *trans* dumbbell of **1** were observed. The *cis* dumbbell is a V-shaped molecule, with a torsion angle of 108° and a *P* value of 0.55, which is much large

than that of the *trans* dumbbell, 0.40. In the proposed packing model in Figure 8c, two *cis* dumbbells can strongly interact with each other through hydrophobic interactions and π – π stacking of adjacent heteroaromatic rings, yielding inter-POM distances of >2 nm, enabling two possible packing modes of *cis* dumbbell to form vesicles: first, a monolayer structure, where two polar head groups of **1** are located on the outer and inner surfaces, respectively, with the linkers forming the solvophobic layer of the vesicle, and second, a bilayer structure, where the two polar heads are on the *same* surface with the linkers residing inside the vesicle shell. The “bent” feature of the *cis*-dumbbell prefers the bilayer model of vesicles because of the easiness of packing; however, we cannot rule out the possibility of the monolayer vesicle model. The well-established theory suggests that a surfactant with packing parameter 0.5–1.0 is able to assemble into bilayer structures. The *cis*-dumbbell has a packing parameter of 0.55 and is therefore more likely to form bilayer vesicles.

CONCLUSIONS

In summary, we have shown that the bipyridine-based dumbbell-shaped POM hybrid **1**, the first POM-based metal-ion-driven molecular switch, can be switched via the addition and removal of Zn^{2+} , which in turn can dramatically change the supramolecular aggregation of the clusters. The hybrid exists as the *trans* dumbbell in metal ion-free solutions and can be converted to the *cis* dumbbell upon the coordination of Zn^{2+} , and this is fully reversible, switching the conformation of the hybrid cluster over multiple cycles with controlled addition and removal of Zn^{2+} ions in a DMSO solution of the hybrid. A multiresponsive switching behavior is observed during the transformation process and the transformation can be further utilized to manipulate its self-assembly behavior, which is believed to mimic the behavior of metal ion-directed folding and assembly process of proteins. The current study could be helpful in not only understanding the metal ion-controlled folding and assembly behavior of biomacromolecules and designing protein-mimic smart molecules with controlled folding and self-assembly behavior but also developing POM-based materials with tunable/modified properties (e.g., catalytic properties and encapsulation/delivery).

EXPERIMENTAL SECTION

Single-Crystal X-ray Diffraction. A sample of **1** was dissolved in dimethylformamide and subjected to partial cation exchange (TBA^+ to H^+) using Amberlite 15 cation exchange resin. Vapor diffusion of diethyl ether into the solution yielded single crystals, one of which was selected and mounted onto a rubber loop using Fomblin oil. X-ray diffraction intensity data were collected at 150(2) K on a Bruker Apex II Quasar CCD diffractometer ($\lambda_{\text{Mo-K}\alpha} = 0.71073 \text{ \AA}$) equipped with a graphite monochromator. Structure solution and refinement were carried out with SHELXS-97⁵⁴ and SHELXL-97⁵⁵ via WinGX⁵⁶ interface. The main dumbbell clusters were well-defined during structure refinement, but the tetrabutylammonium cations were only partially modeled with parts missing in the deep solvent area. Platon SQUEEZE⁵⁷ procedure has been applied to the structure data to improve the structure quality and to determine the solvent void volume of the crystal lattice.

Crystal data and structure refinements for $(\text{C}_{16}\text{H}_{36}\text{N})_{10}\text{H}_2[\{\text{P}_2\text{V}_3\text{W}_{15}\text{O}_{59}(\text{OCH}_2)_3\text{CNHCO}\}_2\text{C}_{10}\text{H}_6\text{N}_2]:\text{C}_{180}\text{H}_{382}\text{N}_{14}\text{O}_{126}\text{P}_4\text{V}_6\text{W}_{30}$, $F_w = 10704.02 \text{ g mol}^{-1}$; orange block crystal $0.12 \times 0.06 \times 0.03 \text{ mm}^3$. Monoclinic, space group $P2_1/n$, $a = 15.4135(5)$, $b = 28.3495(10)$, $c = 34.4392(12) \text{ \AA}$, $\beta = 93.178(2)^\circ$, $V = 15025.6(9) \text{ \AA}^3$, $Z = 2$, $\rho = 2.366 \text{ g cm}^{-3}$, $\lambda(\text{Mo K}\alpha) = 0.71073$, 84776 reflections measured, 23950 unique ($R_{\text{int}} = 0.1054$), which were used

in all calculations. Final R1 = 0.0822 and wR2 = 0.2384 (all data). CCDC reference number CCDC 936592.

SAXS Experimental Section. The SAXS experiments were performed at 12-ID-B station with X-ray energy of 12 keV at the Advanced Photon Source of the Argonne National Laboratory. The sample to detector distance was about 2 m. A Pilatus detector (Dectris Ltd.) was used to acquire images with typical exposure times in the range of 1.0 s.

TEM. The TEM images were taken on a JEOL JEM-2000 electron microscope operated at 200 kV. Samples for the TEM analysis were prepared by dropping a small volume of the solution sample onto a holey carbon film on copper grid. EDS experiments were carried out under the same condition with EDS attachments (Oxford) in JEM-2000.

Static Light Scattering. A commercial Brookhaven Instrument LLS spectrometer equipped with a solid-state laser operating at 532 nm was used for measurement of both SLS and DLS. SLS experiments were performed at scattering angles (θ) between 20° and 100°, at 2° intervals. However, due to the large fluctuations in scattered intensities at low scattering angles, we removed the data from 20° to 40° in the final analysis. Derived from the Rayleigh–Gans–Debye equation,⁵⁸ a partial Zimm plot was used to analyze the SLS data to obtain the radius of gyration (R_g). The partial Zimm plot stems from the following approximate formula: $1/I = C(1 + R_g^2(q^2/3))$. Here R_g is determined from the slope and the intercept of a plot of $1/I$ vs q^2 .

Dynamic Light Scattering. DLS measures the intensity–intensity time correlation function by means of a BI-9000AT multichannel digital correlator. The field correlation function $g^{(1)}(\tau)$ was analyzed by the constrained regularized CONTIN method⁵⁹ to yield information on the distribution of the characteristic line width Γ . The normalized distribution function of the characteristic line width, $G(\Gamma)$, so obtained, can be used to determine an average apparent translational diffusion coefficient, $D_{app} = \Gamma/q^2$. The hydrodynamic radius, R_h , is related to D via the Stokes–Einstein equation: $R_h = kT/(6\pi\eta D)$ where k is the Boltzmann constant and η the viscosity of the solvent at temperature T . From DLS measurements, we can obtain the particle-size distribution in solution from a plot of $\Gamma G(\Gamma)$ versus R_h . The R_h of the particles is obtained by extrapolating $R_{h,app}$ to zero scattering angle.

1D NMR and 2D COSY, DOSY, and NOESY NMR Experiments. All the NMR spectra were recorded on Bruker Avance 500 MHz spectrometer equipped with a BBO probe at 298 K. Two-dimensional COSY spectra were collected under standard conditions. Two-dimensional NOESY were performed with mixing times ranging from 50 to 500 ms. The appropriate mixing time for *trans* dumbbell and *cis* dumbbell solution were determined to be 70 and 300 ms.

DOSY was performed on a Bruker Avance 500 MHz spectrometer with the magnetic field gradient (g) varying from 0 to 32 G/cm in 16–32 steps. The length of the gradient (δ) was from 6000 to 8000 ms, and the time interval between two pulsed gradients (Δ) was from 0.1 to 0.15 s. All spectra were taken at room temperature. After the data collection, FIDs were processed and analyzed with the NMR software TopSpin 2.0 provided by Bruker. Both T1/T2 relaxation and CONTIN methods were used to fit the raw data. The observed proton signal I in a standard DOSY spectrum is expressed through eq 1:

$$I = I_0 \exp \left[-(2\pi\gamma\delta)^2 \left(\Delta - \frac{\delta}{3} \right) D g^2 \right] \quad (1)$$

where I_0 is the reference intensity and γ is the gyromagnetic ratio of the proton. If only one diffusive component exists in the solution, a straight line will occur in a plot of $\ln(I/I_0)$ versus g^2 , and the apparent diffusion coefficient (D) can be calculated from the slope using linear regression analysis.

■ ASSOCIATED CONTENT

Supporting Information

All experimental details, Figure S1–S11, single crystal data, and video. This material is available free of charge via the Internet at <http://pubs.acs.org>.

■ AUTHOR INFORMATION

Corresponding Authors

tliu@uakron.edu

lee.cronin@glasgow.ac.uk

Notes

The authors declare no competing financial interest.

■ ACKNOWLEDGMENTS

T. Liu acknowledges support from the NSF (Grant CHE1026505), the A. P. Sloan Foundation, and Lehigh University. L. Cronin acknowledges support from EPSRC and WestCHEM. T. Li and X. Zuo are thankful for the use of the Advanced Photon Source, an Office of Science User Facility operated for the U.S. Department of Energy (DOE) Office of Science by Argonne National Laboratory, supported by the U.S. DOE under Contract No. DE-AC02-06CH11357.

■ REFERENCES

- (1) Kay, E. R.; Leigh, D. A.; Zerbetto, F. *Angew. Chem., Int. Ed.* **2007**, *46*, 72.
- (2) Coskun, A.; Banaszak, M.; Astumian, R. D.; Stoddart, J. F.; Grzybowski, B. A. *Chem. Soc. Rev.* **2012**, *41*, 19.
- (3) Tian, H.; Yang, S. *Chem. Soc. Rev.* **2004**, *33*, 85.
- (4) Saha, S.; Stoddart, J. F. *Chem. Soc. Rev.* **2007**, *36*, 77.
- (5) Raymo, F. M.; Tomasulo, M. *Chem. Soc. Rev.* **2005**, *34*, 327.
- (6) Tian, H.; Wang, Q.-C. *Chem. Soc. Rev.* **2006**, *35*, 361.
- (7) Klajn, R.; Stoddart, J. F.; Grzybowski, B. A. *Chem. Soc. Rev.* **2010**, *39*, 2203.
- (8) Otsuki, J.; Akasaka, T.; Araki, K. *Coord. Chem. Rev.* **2008**, *252*, 32.
- (9) Champin, B.; Mobian, P.; Sauvage, J.-P. *Chem. Soc. Rev.* **2007**, *36*, 358.
- (10) Elhabiri, M.; Albrecht-Gary, A.-M. *Coord. Chem. Rev.* **2008**, *252*, 1079.
- (11) Browne, W. R.; Feringa, B. L. *Nat. Nanotechnol.* **2006**, *1*, 25.
- (12) Feringa, B. L. *Acc. Chem. Res.* **2001**, *34*, 504.
- (13) *Molecular Switches*, 2nd ed.; Feringa, B. L., Browne, W. R., Eds.; Wiley-VCH: Weinheim, Germany, 2011; Vol. 1.
- (14) Feringa, B. L.; van Delden, R. A.; Koumura, N.; Geertsema, E. M. *Chem. Rev.* **2000**, *100*, 1789.
- (15) Amendola, V.; Fabbrizzi, L.; Mangano, C.; Pallavicini, P. *Acc. Chem. Res.* **2001**, *34*, 488.
- (16) Fabbrizzi, L.; Licchelli, M.; Pallavicini, P. *Acc. Chem. Res.* **1999**, *32*, 846.
- (17) *Metal Ions in Biology and Medicine*; Centeno, J. A., Collery, P., Vernet, G., Finkelman, R. B., Gibb, H., Etienne, J., Eds.; John Libbey Eurotext: Paris, France, 2000; Vol. 6.
- (18) Jiang, Y.; Lee, A.; Chen, J.; Cadene, M.; Chait, B. T.; MacKinnon, R. *Nature* **2002**, *417*, 515.
- (19) Salgado, E. N.; Radford, R. J.; Tezcan, F. A. *Acc. Chem. Res.* **2010**, *43*, 661.
- (20) *Protein Folding and Metal Ions: Mechanisms, Biology and Disease*; Gomes, C. M., Wittung-Stafshede, P., Eds.; CRC Press: Boca Raton, FL, 2011.
- (21) Hill, C. L. *Chem. Rev.* **1998**, *98*, 1.
- (22) Long, D.-L.; Burkholder, E.; Cronin, L. *Chem. Soc. Rev.* **2007**, *36*, 105.
- (23) Long, D.-L.; Tsunashima, R.; Cronin, L. *Angew. Chem., Int. Ed.* **2010**, *49*, 1736.
- (24) Proust, A.; Thouvenot, R.; Gouzerh, P. *Chem. Commun.* **2008**, 1837.

- (25) Thiel, J.; Yang, D.; Rosnes, M. H.; Liu, X.; Yvon, C.; Kelly, S. E.; Song, Y.-F.; Long, D.-L.; Cronin, L. *Angew. Chem., Int. Ed.* **2011**, *50*, 8871.
- (26) Yan, Y.; Wang, H.; Li, B.; Hou, G.; Yin, Z.; Wu, L.; Yam, V. W. *W. Angew. Chem., Int. Ed.* **2010**, *49*, 9233.
- (27) Oms, O.; Hakouk, K.; Dessapt, R.; Deniard, P.; Jobic, S.; Dolbecq, A.; Palacin, T.; Nadjjo, L.; Keita, B.; Marrot, J.; Mialane, P. *Chem. Commun.* **2012**, *48*, 12103.
- (28) Li, H.; Pang, S.; Wu, S.; Feng, X.; Müllen, K.; Bubeck, C. *J. Am. Chem. Soc.* **2011**, *133*, 9423.
- (29) Yang, Y.; Xu, L.; Li, F.; Du, X.; Sun, Z. *J. Mater. Chem.* **2010**, *20*, 10835.
- (30) Rieger, J.; Antoun, T.; Lee, S.-H.; Chenal, M.; Pembouong, G.; Lesage de la Haye, J.; Azcarate, I.; Hasenknopf, B.; Lacôte, E. *Chem.—Eur. J.* **2012**, *18*, 3355.
- (31) Yin, P.; Wu, P.; Xiao, Z.; Li, D.; Bitterlich, E.; Zhang, J.; Cheng, P.; Vezenov, D. V.; Liu, T.; Wei, Y. *Angew. Chem., Int. Ed.* **2011**, *50*, 2521.
- (32) Li, D.; Song, J.; Yin, P.; Simotwo, S.; Bassler, A. J.; Aung, Y.; Roberts, J. E.; Hardcastle, K. I.; Hill, C. L.; Liu, T. *J. Am. Chem. Soc.* **2011**, *133*, 14010.
- (33) Yin, P.; Jin, L.; Li, D.; Cheng, P.; Vezenov, D. V.; Bitterlich, E.; Wu, X.; Peng, Z.; Liu, T. *Chem.—Eur. J.* **2012**, *18*, 6754.
- (34) Pradeep, C. P.; Li, F.-Y.; Lydon, C.; Miras, H. N.; Long, D.-L.; Xu, L.; Cronin, L. *Chem.—Eur. J.* **2011**, *17*, 7472.
- (35) Haberhauer, G. *Angew. Chem., Int. Ed.* **2010**, *49*, 9286.
- (36) Zahn, S.; Reckien, W.; Kirchner, B.; Staats, H.; Matthey, J.; Lützen, A. *Chem.—Eur. J.* **2009**, *15*, 2572.
- (37) Plitt, P.; Gross, D. E.; Lynch, V. M.; Sessler, J. L. *Chem.—Eur. J.* **2007**, *13*, 1374.
- (38) König, B.; Hollnagel, H.; Ahrens, B.; Jones, P. G. *Angew. Chem., Int. Ed.* **1995**, *34*, 2538.
- (39) Pradeep, C. P.; Misdrahi, M. F.; Li, F.-Y.; Zhang, J.; Xu, L.; Long, D.-L.; Liu, T.; Cronin, L. *Angew. Chem., Int. Ed.* **2009**, *48*, 8309.
- (40) Li, T.; Winans, R. E.; Lee, B. *Langmuir* **2011**, *27*, 10929.
- (41) Macfarlane, R. J.; Lee, B.; Jones, M. R.; Harris, N.; Schatz, G. C.; Mirkin, C. A. *Science* **2011**, *334*, 204.
- (42) Antonio, M. R.; Nyman, M.; Anderson, T. M. *Angew. Chem., Int. Ed.* **2009**, *48*, 6136.
- (43) Pigga, J. M.; Kistler, M. L.; Shew, C. Y.; Antonio, M. R.; Liu, T. *Angew. Chem., Int. Ed.* **2009**, *48*, 6538.
- (44) Kojima, T.; Antonio, M. R.; Ozeki, T. *J. Am. Chem. Soc.* **2011**, *133*, 7248.
- (45) Svergun, D. *J. Appl. Crystallogr.* **1992**, *25*, 495.
- (46) Svergun, D. I.; Koch, M. H. J. *Rep. Prog. Phys.* **2003**, *66*, 1735.
- (47) Zuo, X.; Cui, G.; Merz, K. M.; Zhang, L.; Lewis, F. D.; Tiede, D. M. *Proc. Natl. Acad. Sci. U.S.A.* **2006**, *103*, 3534.
- (48) Zhang, R.; Thiyagarajan, P.; Tiede, D. M. *J. Appl. Crystallogr.* **2000**, *33*, 565.
- (49) Ernst, R. R.; Bodenhausen, B.; Wokaun, A. *Principles of Nuclear Magnetic Resonances in One or Two Dimensions*; Oxford University Press: Cambridge, 1992.
- (50) Misdrahi, M. F.; Wang, M.; Pradeep, C. P.; Li, F.-Y.; Lydon, C.; Xu, L.; Cronin, L.; Liu, T. *Langmuir* **2011**, *27*, 9193.
- (51) Yin, P.; Li, D.; Liu, T. *Chem. Soc. Rev.* **2012**, *41*, 7368.
- (52) Nagarajan, R. *Langmuir* **2001**, *18*, 31.
- (53) Butt, H.-J.; Graf, K.; Kappl, M. In *Physics and Chemistry of Interfaces*; Wiley-VCH Verlag GmbH & Co. KGaA: Weinheim, Germany, 2004; p 246.
- (54) Sheldrick, G. *Acta Crystallogr., Sect. A: Found. Crystallogr.* **1990**, *46*, 467.
- (55) Sheldrick, G. *Acta Crystallogr., Sect. A: Found. Crystallogr.* **2008**, *64*, 112.
- (56) Farrugia, L. *J. Appl. Crystallogr.* **1999**, *32*, 837.
- (57) Sluis, P. v. d.; Spek, A. L. *Acta Crystallogr., Sect. A: Found. Crystallogr.* **1990**, *46*, 194.
- (58) Hiemenz, P. C.; Rajagopalan, R. *Principles of Colloid and Surface Chemistry*; Marcel Dekker: New York, 1997.
- (59) Provencher, S. W. *Comput. Phys. Commun.* **1982**, *27*, 229.